MIMO CPW-Fed Bent Antenna Based USB Dongle for ECMA-368 WPANs

Yazid Beddiafi[1], Djamel Abed[2], Ahcene Boualleg[1] and Elhadi Mehallel[2,3]
[1]Telecommunications Laboratory, Université 8 mai 1945 Guelma, Algeria
[2]LabCAV Laboratory, Université 8 mai 1945 Guelma, Algeria
[3]Université Ziane Achour Djelfa, Algeria

Corresponding author: Yazid Beddiafi (e-mail: beddiafi.yazid@univ-guelma.dz)

ABSTRACT A multiple-input-multiple-output (MIMO) ultra-wideband (UWB) printed bent antenna, suitable for MB-OFDM ECMA-368 system integration with the wireless universal serial-bus (WUSB) dongle is proposed. The antenna is made up of two antenna components that have a total area of 18×53 mm^2. Each antenna element is a simple modified folded-monopole, with a coplanar waveguide (CPW) feeds. The design process of proposed MIMO UWB CPW-fed bent antenna configuration is presented in four simple steps. Experimental results show that the proposed design has a good impedance bandwidth in the range of 2.95–18.55 GHz with 147.2% fractional bandwidth (FBW). Moreover, the proposed antenna enjoys, low envelope correlation coefficient (ECC), good diversity gain (DG), low total active reflection coefficient (TARC) and omnidirectional radiation patterns. The bit error rate (BER) of the overall MB-OFDM ECMA-368 system with the existence of the proposed MIMO UWB CPW-fed bent antenna is evaluated in more realistic transmission channel scenario by using the extracted transmitting and receiving UWB antennas transfer functions.

INDEX TERMS MB-OFDM, ECMA-368, MIMO UWB antenna, UWB WUSB dongle.

I. INTRODUCTION

Sharing information very quickly with a high data rate is an obsession of all humanity in the world, following this reason, the presence of large bandwidth is inevitable. Ultra-wideband (UWB) technology used in wireless communication systems has been widely investigated for its low cost, high data transmission rates, low power and acceptable physical implementation [1]-[3]. In UWB two high data rate techniques are possible, direct sequence UWB (DS-UWB) [4] and multiband orthogonal frequency division multiplexing (MB-OFDM) [5][6]. MB-OFDM, which is supposed to deliver data speeds of up to 480 Mb/s, gained significant interest due to its potential to minimize multipath and radio frequency interference effects [7][8], it has been oriented to differentes standards such as IEEE 802.15.3a and ECMA-368 [5][6]. MB-OFDM in combination with multi-input multi-output (MIMO) techniques has shown to be an effective solution for the short-range communication limitations that need devices transmitting at extremely low power levels, following the federal communication commission (FCC) approval in the band 3.1 GHz to 10.6 GHz [9][10][11]. For this purpose MIMO UWB antennas are recently developed. In [12], a MIMO UWB antenna with an inverted Y-shaped stub was studied. The antenna presents an impedance bandwidth of 7.4 GHz from 3.2 to 10.6 GHz, with a $40 \text{ mm} \times 68 \text{ mm}$ overall dimension. To achieve excellent isolation, an F-shaped stub was utilized in a MIMO UWB antenna in [13]. The antenna's impedance bandwidth is 12 GHz in the $2.5 - 14.5$ GHz range, with DG more than 7.4 and ECC smaller than 0.04. The antenna's dimensions are $50 \text{ mm} \times 30 \text{ mm}$. A rectangular-shaped MIMO UWB antenna was studied in [14]. The -10 dB $|S_{11}|$ bandwidth does not encompass the desired UWB spectrum and the antenna was $27 \text{ mm} \times 47 \text{ mm}$. In [15] a $40 \text{ mm} \times 80 \text{ mm}$ MIMO UWB antenna based on metamaterial rectangular loop resonator is proposed. The impedance bandwidth is $4.5 - 8$ GHz, the ECC is less than 0.02, and DG is approximately 10 dB. In [16] a $50 \text{ mm} \times 82 \text{ mm}$ MIMO UWB antenna is proposed based-on T-shaped isolation stub. A U-shaped MIMO UWB antenna with comb-line-shaped stub is proposed in [17]. The physical size of this antenna is $26 \text{ mm} \times 31 \text{ mm}$ with an impedance bandwidth of 9.1 GHz in frequency range 2.9 - 12 GHz. In [18] a $22 \text{ mm} \times 31 \text{ mm}$ MIMO UWB antenna based on T-shaped stub is studied. The impedance bandwidth is 9.1 GHz frequency range $2.9 - 12$ GHz. Based on stepped slots four elements MIMO UWB antenna is proposed in [19]. The impedance bandwidth of the presented antenna is $3.1 - 12$ GHz and the ECC is less than 0.5. A circular-shaped MIMO UWB antenna is investigated in [20]. The antenna size $4 \text{ cm} \times 4 \text{ cm}$ with an operating band from 3.1 to 11 GHz. In [21], a $26 \text{ mm} \times 55 \text{ mm}$ MIMO UWB antenna with a half-circular form is presented for an operating band from 3.1 to 12.3 GHz. In [22], another isolation T-shaped stub is introduced in a MIMO UWB antenna structure,

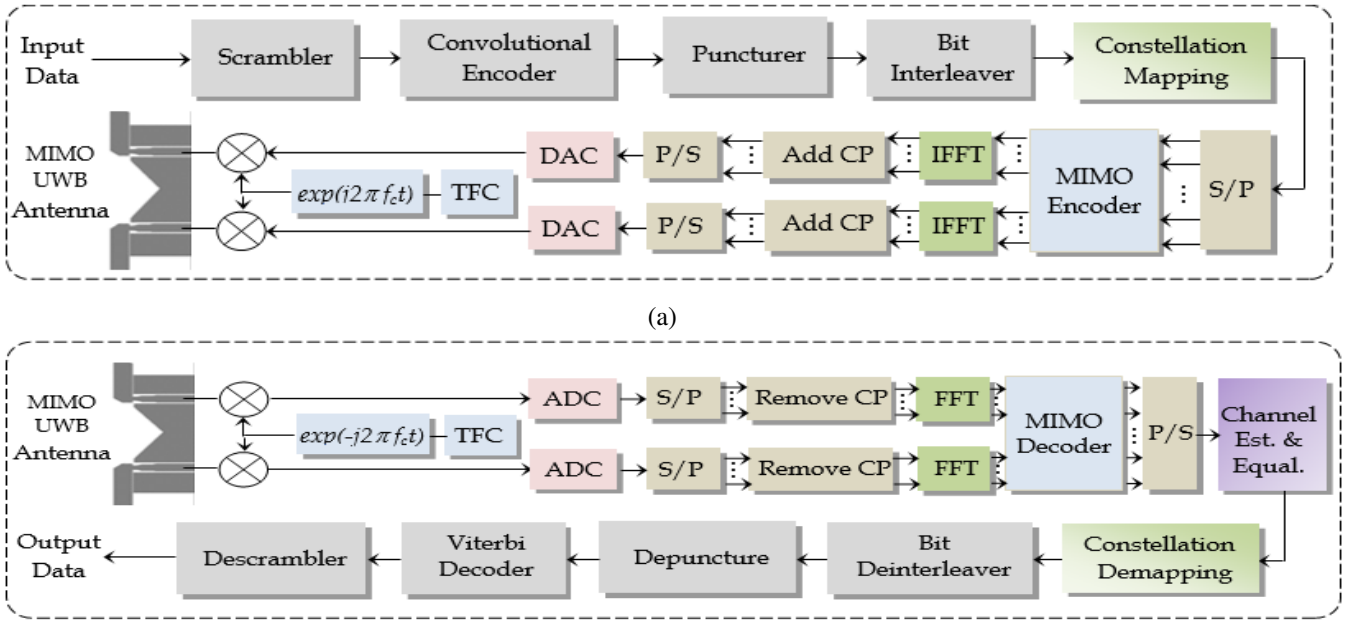

FIGURE 1: The MIMO ECMA-368 MB-OFDM communication system with the proposed MIMO UWB antenna (a) The transmitter (b) The receiver

the overall antenna size is $26\ \text{mm} \times 28\ \text{mm} \times 0.8\ \text{mm}$. In [23], a rectangular shape MIMO UWB antenna with two isolation structures is studied. The antenna dimensions are $25\ \text{mm} \times 38\ \text{mm}$ and the -10 dB $|S_{11}|$ bandwidth is between 2.2 and 10.8 GHz. In [24] a $35\ \text{mm} \times 68\ \text{mm}$ single stub circular-shaped MIMO UWB antenna is designed. In that design, the antenna impedance bandwidth is 7.55 GHz, operating in the frequency band from 3.1 to 10.65 GHz. A new T-shaped isolation stub for a rectangular MIMO UWB antenna is described in [25] with a dimension of $22\ \text{mm} \times 36\ \text{mm}$ and an ECC less than 0.1. This antenna functioned in the frequency range of 3.1 to 11 GHz. In [26] $30 \times 30 \times 0.8\ \text{mm}^3$ MIMO UWB antenna is designed based on a stepped-shaped ground stub. The antenna impedance bandwidth is 7.9 GHz in frequency range from $3.08 - 10.98$ GHz. The DG and the ECC are 9.51 dB, and less than 0.013, respectively. In [27], semi-circle-shaped MIMO UWB antenna is proposed. The antenna size was $41 \times 30\ \text{mm}^2$ with an impedance bandwidth from 3.04-10.87 GHz. An E-shaped slot is inserted in the radiating patch to achieve a high isolation. In [28], a $39.6 \times 29 \times 5\ \text{mm}^3$ MIMO UWB antenna with two rack-shaped radiator elements with an impedance bandwidth ranging from 3.54-10.89 GHz, the DG is superior to 9.93 dB and the ECC is lower than 0.0059. In [29], the authors proposed a $21 \times 34 \times 1.6\ \text{mm}^3$ MIMO UWB antenna with an impedance bandwidth of 5.73 GHz in frequency range from 3.62 to 9.35 GHz. A MIMO UWB antenna for the GSM band is constructed in [30], with unit cell of $36 \times 45 \times 1.6\ \text{mm}^3$. The antenna impedance bandwidths are 9.49 GHz, and 0.26 GHz for UWB and GSM, respectively. The maximal peak gain is about 8.48dBi, and ECC is less than 0.025. Others MIMO UWB antenna designs are given in [31]-[37]

This paper firstly reviews the literature related to the MB-OFDM physical layer through the ECMA-368 standard. Secondly, a MIMO UWB printed bent antenna is designed starting from the conventional monopole in four simple steps. The designed antenna is suitable for integration with the wireless universal serial-bus (WUSB) dongle. The antenna consists of two elements with an overall area of $18 \times 53\ \text{mm}^2$. Each antenna element is a simple modified folded-monopole fed by a coplanar waveguide (CPW). The isolation stub technique is avoided in this design and replaced by triangular-shaped notched ground-plane for antennas decoupling control. Numerical and experimental results appearance that the proposed design has a wideband impedance matching covering the 3.1-10.6 GHz ECMA-368 UWB band with a low ECC, a good DG, a low TARC and an omnidirectional radiation patterns. In the last part of the paper, the model of proposed MIMO UWB is added to the system model and global system simulations are performed.

II. THE ECMA-368 STANDARD

The overall MIMO-UWB system discussed in this section is given in Figures 1*a* and 1*b*. The MB-OFDM UWB system uses a frame-based transmission, which follows the ECMA-368 standard. As shown in Figure 2 the frame structure consists of a preamble used for synchronization and/or channel estimation and a header which contains information regarding the frame setup. The information symbols are included in the payload part. Convolutional encoder is

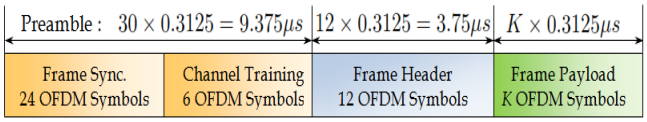

FIGURE 2: The frame structure of The MB-OFDM through the ECMA-368 standard ECMA-368 standard.

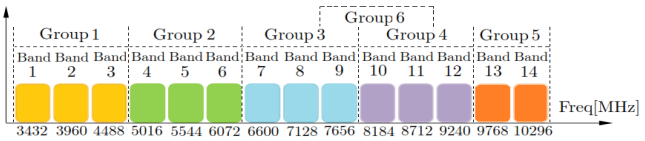

FIGURE 3: The MB-OFDM band groups through the ECMA-368 standard.

adopted as Forward Error Corrections (FEC) in ECMA-368, $R = 1/3$ coding rate is used and three octal generator polynomials with $g_0 = 133_8$, $g_1 = 165_8$ and $g_2 = 171_8$ octal polynomials generator. Puncturing technique is used to determine additional rates ($1/2$, $5/8$ and $3/4$). After coding and padding operations, bit interleaving is applied to offer resilience against burst faults. This process contains three phases, *i*) symbol interleaving, *ii*) intra-symbol tone interleaving and *iii*) intra-symbol cyclic shifts [38]. The coded bits are within blocks of N_{CBPS} bits for symbol interleaving. The output is provided by

$$a_s[i] = a\left[\lfloor \tfrac{i}{N_{\mathrm{CBPS}}} \rfloor + (\tfrac{6}{N_{\mathrm{TDS}}}) \times mod(i,\ N_{\mathrm{CBPS}})\right] \quad (1)$$

where $\lfloor . \rfloor$ is the floor function, $a[i]$ is the input bits and $mod(a, b)$ denotes the modulus operator. A standard intra-symbol interleaver block is then used to permute the sequence $a_s\,[i]$. The tone interleaver's output is given by

$$a_T\,[j] = a_s\left[\left\lfloor \frac{j}{N_{\mathrm{T}_{int}}} \right\rfloor + 10 \times mod\,(j,\ N_{\mathrm{T}_{int}})\right] \quad (2)$$

The tone interleaver's output is then sent into an intra-symbol cyclic shifter. The output result is as follows

$$b[i] = a_T[m(i) + N_{\mathrm{CBPS}} + mod(i + \ m\,(i) \times N_{cyc}, N_{\mathrm{CBPS}})] \quad (3)$$

where $m(i) = \lfloor i/N_{\mathrm{CBPS}} \rfloor$ and $i = 0, \ldots, N_{\mathrm{CBPS}} - 1$. The binary data stream is projected into a complex constellation after interleaving. 53.3, 80, 106.7, 160, 200, 320, 400 and 480 Mb/s are the data rates used by ECMA-368. The quadrature phase-shift keying (QPSK) constellation is used for data speeds of 53.3 to 200 Mb/s. For data rates between 320 and 480 Mb/s, the binary data is mapped onto a multi-dimensional constellation using a dual-carrier modulation (DCM) technique. In QPSK modulation the interleaved binary data is divided into groups of two bits and mapped according to the Gray-coding using the equation

$$D_{\mathrm{QPSK}}[K] = \mathrm{F}_{\mathrm{MOD}} \times [(2 \times b(2K) - 1) + j(2 \times b[2K+1] - 1)] \quad (4)$$

$D_{\mathrm{QPSK}}\,[K]$ denotes the output bits, $\mathrm{F}_{MOD} = 1/\sqrt{2}$ is the normalization factor and $b[2K]$ is the input bits. The interleaved bits are split into groups of 200 bits in DCM modulation, and then into 50 groups of four bits. In the same way as in reference [38], we have $b[g(n)]$, $b[g(n)+1]$, $b[g(n) + 50]$, $b[g(n) + 51]$ where $g(n)$ is expressed as

$$g(n) = \begin{cases} 2n & n \in \{0, 1, \ldots, 24\} \\ 2n + 50 & n \in \{25, \ldots, 49\} \end{cases} \quad (5)$$

$x[g(n)] + j\ x[g(n) + 50]$, $x[g(n) + 1] + j\ x[g(n) + 51]$ are the two QPSK symbols formed by each set of four binary bits. The DCM modulation is then utilizes a matrix H to construct the two DCM symbols from of the two QPSK symbols which are combined to produce two 16QAM [39] as given in Equations (6), (7) and (8).

$$\begin{bmatrix} x_{g(n)} + jx_{g(n)+50} \\ x_{g(n)+1} + jx_{g(n)+51} \end{bmatrix} = \begin{bmatrix} (2b_{g(n)} - 1) \\ (2b_{g(n)+1} - 1) \end{bmatrix} + \begin{bmatrix} j(2b_{g(n)+50} - 1) \\ j(2b_{g(n)+51} - 1) \end{bmatrix}. \quad (6)$$

$$H = \begin{bmatrix} 2 & 1 \\ 1 & -2 \end{bmatrix} \quad (7)$$

$$\begin{bmatrix} y_{DCM}(n) \\ y_{DCM}(n+50) \end{bmatrix} = \tfrac{1}{\sqrt{10}} \begin{bmatrix} 2 & 1 \\ 1 & -2 \end{bmatrix} \times \begin{bmatrix} x_{g(n)} + jx_{g(n)+50} \\ x_{g(n)+1} + jx_{g(n)+51} \end{bmatrix} \quad (8)$$

13 pilot subcarriers among all the subcarriers are used. The values of pilot subcarriers are determined by the data rates.

$$d_{pilot}[l] = \begin{cases} \frac{1-j}{\sqrt{2}} & l = 0, 3, & 53.3, 80\mathrm{Mb/s} \\ \frac{-1+j}{\sqrt{2}} & l = 1, 2, 4, 5, & 53.3, 80\mathrm{Mb/s} \\ \frac{1+j}{\sqrt{2}} & l = 8, 11, & 53.3, 80\mathrm{Mb/s} \\ \frac{-1-j}{\sqrt{2}} & l = 6, 7, 9, 10, & 53.3, 80\mathrm{Mb/s} \\ \frac{1+j}{\sqrt{2}} & l = 0, 3, 8, 11, & > 80\mathrm{Mb/s} \\ \frac{-1-j}{\sqrt{2}} & l = 1, 2, 4, 5, 6, 7, 9, 10, & > 80\mathrm{Mb/s} \end{cases} \quad (9)$$

The normalized complex data symbol sequence is divided into two streams by using 2×2 MIMO coding. At the each IDFT input the MB-OFDM signal may be explained as

$$S_n = \begin{cases} 0 & n = 64 \\ 0 & n = 1, 2, 126, 127, 128 \\ d_{pilot} & n = 9 : 10 : 119 \\ y_{\mathrm{QPSK/DCM}}(n-2) & n = 3, 4, 5, 6, 7 \\ y_{\mathrm{QPSK/DCM}}(n-25) & n = 121 : 1 : 125 \\ y_{\mathrm{QPSK/DCM}} & Otherwise \end{cases} \quad (10)$$

Finally, mathematically at each transmit antenna, the transmitted radio frequency signal $S_{\mathrm{RF}}(t)$ is expressed as

$$S_{\mathrm{RF}}(t) = \Re\left\{\sum_{n=0}^{N_{paket}-1} S_n(t - nT_{\mathrm{SYM}})e^{(j2\pi f_c q(n)t)}\right\} \quad (11)$$

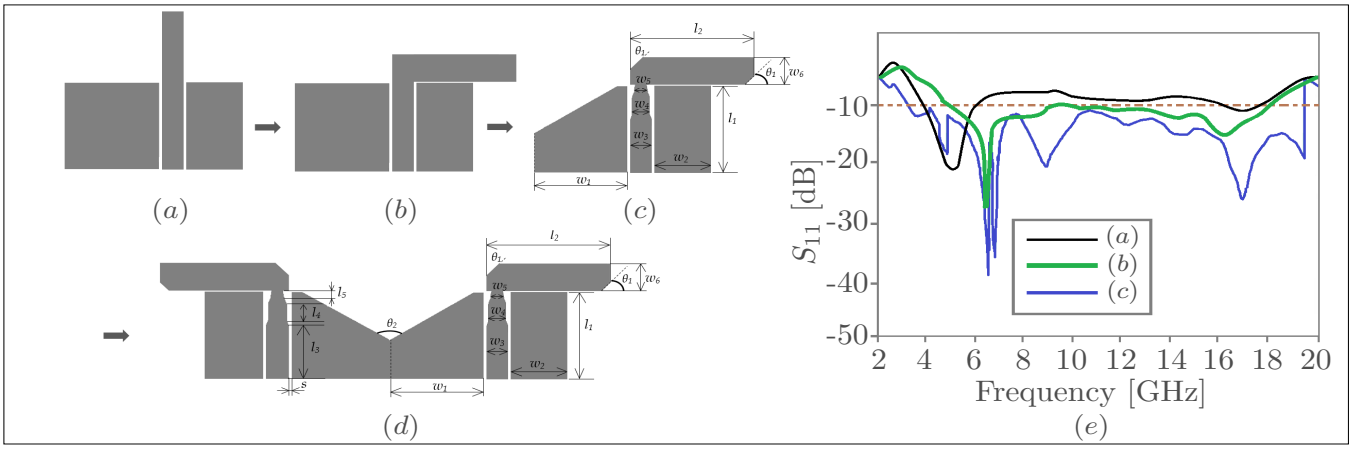

FIGURE 4: The Design steps of the proposed MIMO-UWB antenna (a) Conventional monopole antenna with partial ground plane and asymmetric CPW-fed, (b) The UWB CPW-fed L-shaped (bent) antenna, (c) The modified UWB CPW-fed bent antenna, (d) The proposed MIMO UWB CPW-fed bent antenna, (e) The corresponding S_{11} parameters for (a), (b) and (c) antennas.

Where $\Re\{.\}$ denotes the real part of the transmitted radio frequency signal, T_{SYM} represents the symbol duration, N_{paket} represents the total amount of symbols, f_c is the center frequency, $S_n\,(t)$ denotes the complex baseband signal and $q\,(n)$ is used to transfer the *nth* symbol to the proper frequency. According to the chosen time frequency coding (TFC), the transmitted symbols are interleaved over the 14 bands seen in Figure 3. The central frequency f_c depends on N_b as follows

$$f_c = 2.904 + (N_b \times 528)\,, N_b = 1, \ldots 14 \quad (\mathrm{MHz}) \quad (12)$$

We note that in Equation (11), the information type of each symbol in the baseband signal $S_n(t)$ is related to its location. For each payload N_{Packet} is given by

$$N_{\mathrm{Packet}} = N_{\mathrm{Frame}} + N_{\mathrm{Sync}} + N_{\mathrm{HDR}} \quad (13)$$

Where N_{Frame} presents the number of symbols in the PSDU, N_{Sync} denotes the number of synchronization symbols in the PLCP preamble and N_{HDR} is the number of symbols contained in the PLCP header.

III. ANTENNA DESIGN

The design approach of the proposed MIMO UWB antenna arrangement is depicted in Figure 4. A simple planar monopole antenna is used to create the proposed MIMO UWB configuration. In its conventional shape, the monopole antenna does not meet the UWB specification. In the first step of the proposed design procedure, the rectangular-shaped radiating element is bent to produce an L-shaped strip with a 50 Ω side-plane asymmetric CPW-fed. The asymmetric feeding technique is introduced to increase the impedance bandwidth [1]. In the second step of the design process, the L-shaped strip radiator is modified to create new resonances in the required band and the stepped impedance feeding line is employed in order to enhance impedance matching. Also, the left partial ground plane is modified to corner notched ground plane. At the third step of the design, the second identical radiating element is obtained by using mirror image with 0° orientation. We note the etched triangular-shaped slot on the partial ground plane providing removal of the isolation stub between the two radiating element. By the means of the angle of this triangular-shaped slot sufficient isolation can be maintained between two input ports. The design steps used to obtain the proposed MIMO UWB antenna are given in Figures $4(a)$-$4(d)$. The corresponding S_{11} parameters are shown in Figure $4(e)$. The design was optimized for an FR4 substrate with relative permittivity $\varepsilon_r = 4.4$, a thickness $h = 1.6$ mm and loss tangent $\tan\delta = 0.0017$ using Ansys HFSS simulator and the optimized parameters are tabulated in Table 1.

TABLE 1: Optimum Values of the Design Parameters

Parameter	Value	Parameter	Value
l_1	13.92 mm	w_1	10 mm
l_2	13 mm	w_2	6 mm
l_3	5.92 mm	w_3	2.9 mm
l_4	3.20 mm	w_4	2.4 mm
l_5	1.80 mm	w_5	1.6 mm
s	0.025 mm	w_6	4 mm
θ_1	45°	θ_2	130°

IV. RESULTS AND DISCUSSION

The performance of the antenna was simulated using Ansys HFSS simulator. To validate the simulation results, a prototype was constructed and measured. The measurements were taken using a Rhode and Schwarz® ZNB vector network analyser (VNA). In this section, results are presented and discussed.

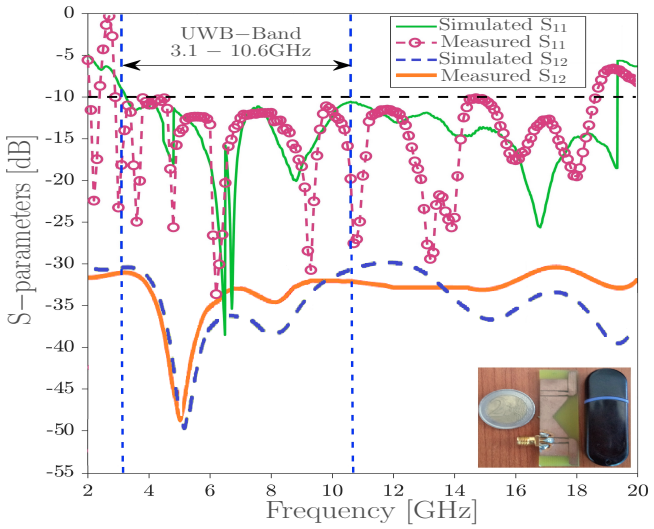

FIGURE 5: Measured and simulated S-parameters of the proposed MIMO UWB CPW-fed bent antenna

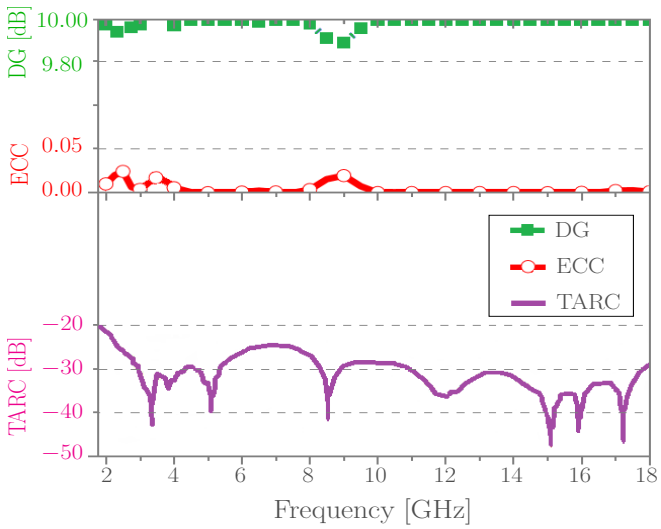

FIGURE 6: Measured ECC, DG and TARC of the proposed MIMO UWB antenna

A. S-PARAMETERS

Figure 4 shows a photograph of the fabricated prototype of the MIMO UWB CPW-fed bent antenna and its simulated/measured S_{11} parameters. The measurements were taken in open laboratory environment using a Rhode and Schwarz® ZNB VNA where one port of the antenna is terminated with a $50\,\Omega$ load and the other port is linked to the VNA. As observed in Figure 5, the simulated and measured results of S_{11} parameters are approximately in good agreement. The S_{11} are ≤ -10 dB over the band from 3.05 to 18.55 GHz which satisfy the MIMO-UWB requirement from 3.1 to 10.6 GHz. Experimental and simulated results of transmission coefficient (S_{21}) show that greater than 25 dB of isolation between the MIMO antenna elements is achieved. It is worth noting that this high isolation between can be controlled easily by using the angle of the etched triangular-shaped slot on the partial ground. The weak variations between simulated and measured results are due to the dielectric imperfections, the fabrication process inaccuracies and the SMA connector solder point losses.

B. DIVERSITY ANALYSIS

In order to assess a MIMO antenna system's diversity performance, some metrics are proposed in the literature to understand the MIMO communication channels characteristics and behavior. To validate the diversity capability of the proposed MIMO UWB CPW-fed bent antenna, the envelope correlation coefficient (ECC), the total active reflection coefficient (TARC), and the diversity gain (DG) properties are the metrics investigated in this paper.

The ECC may be calculated by using scattering parameters or far-field radiation patterns [35][40][45][46]. In this work the ECC metric is obtained from the S-parameters formula given by

$$\mathrm{ECC} = \frac{|S_{11}^{*}S_{12} + S_{21}^{*}S_{22}|^2}{(1-|S_{11}|^2-|S_{21}|^2)(1-|S_{22}|^2-|S_{12}|^2)} \quad (14)$$

The ideal ECC should have a value of zero. In practice, based on the references [36][37] the ECC value < 0.5 is considered to be suitable in MIMO UWB antennas design for diversity applications.

The DG which is required to be varied near 10 dB is given by

$$\mathrm{DG} = 10\sqrt{1-\mathrm{ECC}^2} \quad (15)$$

The measured values ECC and DG metrics as a function of frequency for the proposed the MIMO UWB CPW-fed bent antenna are plotted in Figure 6. It is found that over the entire UWB operating band the ECC remained at a value less than $0,025$ and the DG also remained greater than 9.92 dB. To ensure the efficiency of MIMO antenna TARC is studied. For two port MIMO system, the TARC metric can be calculated from S_{11}, S_{12}, S_{21} and S_{22} by equation given below

$$\mathrm{TARC} = \sqrt{\frac{(S_{11}+S_{12})^2 + (S_{21}+S_{22})^2}{2}} \quad (16)$$

The proposed design has less than -20 dB TARC values as shown in the Figure 6, where the acceptable limits of TARC is < -10 dB. Also, we note that for the proposed MIMO UWB CPW-fed bent antenna the measured peak gain ranges from 0 dBi to 4.2 dBi. The multiplexing efficiency ranging from -1 dB to -3.75 dB over the whole frequency spectrum.

C. RADIATION PATTERNS

The measured 2D-polar far-field radiation patterns of the designed MIMO UWB CPW-fed antenna in co-polarization

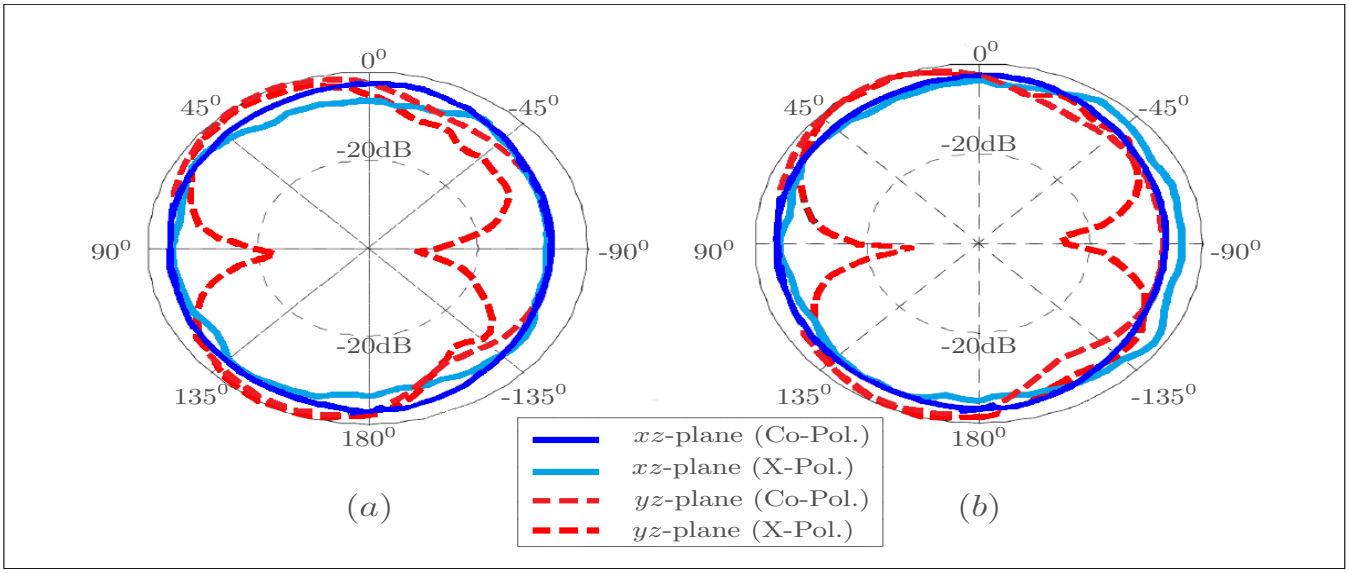

FIGURE 7: The measured far-field co-polarization and cross-polarization radiation pattern of the proposed MIMO UWB CPW-fed bent antenna (a) at 3.5 GHz (b) at 10.6 GHz

and cross-polarization for both the xz-plane (H-plane) and the yz-plane (E-plane) at lower and higher edge frequencies, that are 3.5 GHz and 10.5 GHz, respectively are illustrated in Figures 7. Due to the symmetrical structure of the antenna and the indistinguishable radiated elements port 1 of the connector is taken into account for measurement and port 2 is closed with 50 Ω load. As can see the xz-plane shows nearly omni-directional radiation pattern while yz-plane shows dumbbell-like radiation. In cross-polarization the radiation patterns knew a distortion remarkable in the two planes. We note that the radiation efficiency of the proposed antenna varies between 78% and 95% across the entire UWB band.

The performances of proposed MIMO UWB CPW-fed antenna in terms of antenna size, FBW and ECC are included in Table 2 and compared to previously reported MIMO antenna designs [12]–[37]. It can be seen that the proposed MIMO antenna exhibits good size, higher frequency bandwidth more than 147% FBW. Also, the design has less than 0.025 ECC values at different frequencies.

D. BIT ERROR RATE

In this section, we focus on the BER analysis of the overall MB-OFDM ECMA-368 system with the existence of the proposed antenna in both sides. At the receiver side, the received signal $s_r(t)$ at each antenna output may be produced by convolutioning the input signal with the transmission channel transfer function as

$$s_r(t) = s_t(t) \otimes h(t) \tag{17}$$

The transmission channel transfer function $h(t)$ is given by

$$h(t) = h_{\mathrm{Tx}}(t) \otimes h_{\mathrm{CM}}(t) \otimes h_{\mathrm{Rx}}(t) \tag{18}$$

TABLE 2: A comparison of previously developed MIMO antennas and the proposed antenna

Ref.	Year	Size (mm × mm)	FBW%	ECC
[12]	2011	40 × 68	107.24	–
[13]	2018	50 × 30	141.17	< 0.04
[14]	2013	27 × 47	109.50	< 0.7
[15]	2019	40 × 80	56	< 0.002
[16]	2016	50 × 82	143.23	< 0.0405
[17]	2018	26 × 31	122.14	< 0.001
[18]	2017	22 × 31	122.14	< 0.3
[19]	2015	42 × 25	117.88	< 0.5
[20]	2019	40 × 40	112	< 0.002
[21]	2018	26 × 55	119.5	< 0.1
[22]	2016	26 × 28	115.32	< 0.08
[23]	2015	25 × 38	141	< 0.003
[24]	2017	35 × 68	109.89	< 0.002
[25]	2019	22 × 36	112	< 0.1
[26]	2019	30 × 30	112.37	< 0.0013
[27]	2019	41 × 30	112.58	–
[28]	2020	39.6 × 29	101.87	< 0.0059
[29]	2019	21 × 34	88.35	< 0.005
[30]	2018	36 × 45	122.37	< 0.1
[31]	2015	76.25 × 52.25	120	< 0.05
[32]	2017	72 × 72	107	–
[33]	2015	61 × 68	112	< 0.02
[34]	2016	66.25 × 66.25	120	< 0.005
[35]	2019	36 × 22	113.28	< 0.008
[36]	2020	34 × 34	121	< 0.01
[37]	2021	60 × 35	114	< 0.0035
This Work	2021	18 × 53	147.2	< 0.025

Where $h_{\mathrm{CM}}(t)$ denotes the UWB propagation channel transfer function specified by IEEE 802.15.4a standard [41], $h_{\mathrm{Tx}}(t)$ and $h_{\mathrm{Rx}}(t)$ are the transmitting and the receiving UWB antenna transfer functions, respectively. A good UWB antenna should possess good time delay, low phase distortion and high fidelity [42]. The transfer functions of both the transmitting and receiving antennas are taken in the frequency domain based on the transmission coefficients S_{21} measure-

TABLE 3: Simulation Parameters of the MB-OFDM ECMA-368 system

Parameter	Value
Data rate	53.3, 200 and 480Mbps
Modulation type	QPSK and DCM
Convolutional encoder's rate	1/3, 5/8 and 3/4
Convolutional encoder's constraint length	$K = 7$
Convolutional decoder	Viterbi
Decoding mode	Hard
No. of transmitted MB-OFDM symbols	1200
Total No. of samples/symbol	$N_{\mathrm{SYM}} = 165$
FFT and IFFT size	$N_{\mathrm{FFT}} = 128$
No. of data sub-carriers	$N_{\mathrm{D}} = 100$
No. of pilot sub-carriers	$N_{\mathrm{P}} = 12$
No. of guard sub-carriers	$N_{\mathrm{G}} = 10$
Total No. of sub-carriers	$N_{\mathrm{T}} = 122$
No. of samples in ZPS	$N_{\mathrm{ZPS}} = 37$
No. of channel realizations	100
IEEE Channel model	CM1 and CM2
Type of used MIMO antenna	The proposed antenna
Antennas orientation	$\varphi = 90°, \theta = 0°$

ments. Two identical prototypes of the antenna are deployed in free space and measured with face-to-face orientation and a 60 mm spacing . The frequency domain transfer functions of both the transmitting and receiving antennas are found out from S_{21} measurement as [43][44]

$$H_{\mathrm{Tx}}(\omega,\theta,\varphi) = \sqrt{\frac{j}{2\pi}\left(\frac{\omega}{c}\right)^2 \frac{S_{21}(\omega,\theta,\varphi)}{H_{\mathrm{Ch}(\omega,\theta,\varphi)}}} \tag{19}$$

$$H_{\mathrm{Rx}}(\omega,\theta,\varphi) = \sqrt{\frac{2\pi}{j}\left(\frac{c}{\omega}\right)^2 \frac{S_{21}(\omega,\theta,\varphi)}{H_{\mathrm{Ch}(\omega,\theta,\varphi)}}} \tag{20}$$

The free space transfer function in the frequency domain is denoted by

$$H_{\mathrm{Ch}}(\omega) = \frac{c}{2d\omega}\exp\left(\frac{-j\omega d}{c}\right) \tag{21}$$

where d is the two antennas' separation and c is the velocity. After the antennas characterization, the IDFT is used to transform frequency domain transfer functions to time domain. Once the transmission channel transfer function is extracted the received signals can be easily obtained and after symbols equalization and binarization, the BER of the overall system is calculated. The characteristics of the MB-OFDM ECMA-368 symbols and the simulation parameters are summarized in Table 3.

Figures 8a and 8b illustrates the BER of the overall system with and without the proposed MIMO UWB CPW-fed bent antenna for 53.3, 200 and 480 Mb/s data rates in two channel models CM1 and CM2, respectively. It is shown that in CM1 the BER performance of the overall communication system is sensitive to the antennas existences. It is found that to obtain the ideal performance we need to increase the SNR values by 0.73, 0.65 and 0.53 for the data rates 53.3, 200 and 480 Mb/s, respectively. In CM2, the necessary increase values in SNR are 0.44 and 0.50 for data rates 53.3 and 200 Mb/s, respectively. The obtained BER results with the existence of the proposed MIMO UWB CPW-fed bent antenna are more realistic because it take in consideration the transmitting and receiving UWB antennas transfer functions.

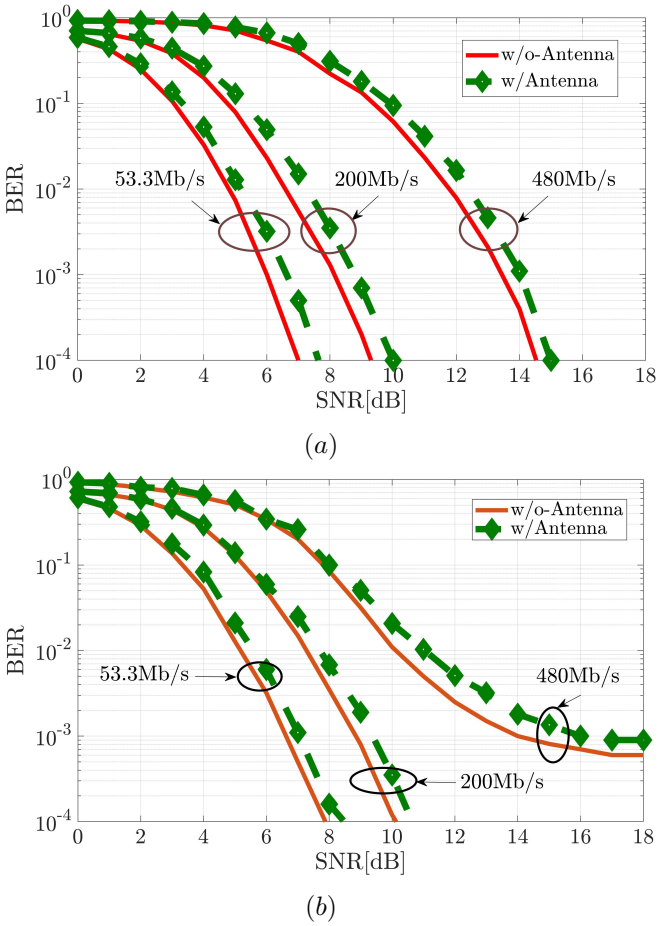

FIGURE 8: BER performance of the the overall system with/without the MIMO CPW-fed bent UWB antenna (a) CM1 case (b) CM2 case

V. CONCLUSIONS

In this research paper, the MB-OFDM physical layer through the ECMA-368 standard is presented and discussed. A new UWB antenna called MIMO CPW-fed Bent antenna is designed, simulated and built. Simulation and measurement results are in good agreement. The antenna impedance bandwidth is 147.2% ranging from 2.95 to 18.55 GHz with a stable radiation pattern. The suggested antenna's diversity performance has also been tested in terms of ECC (≤ 0.025), DG ($\geq$ 9.92 dB) and TARC (≤ -20 dB). Moreover, the BER of the overall MB-OFDM ECMA-368 system with the proposed MIMO UWB CPW-fed bent antenna is evaluated in more realistic transmission channel scenarios. The evaluation process of the overall system demonstrates that the suggested antenna may be utilized for future high data rates MIMO UWB ECMA-368 WPANs applications as an USB dongle.

REFERENCES

[1] Sergio Curto, Matthias John, Max J. Ammann, Groundplane Dependent Performance of Printed Antenna for MB-OFDM-UWB, IEEE 65th Vehicular Technology Conference,22-25 April, Dublin, 2007.

[2] T.S.P. See, Z.N. Chen, An ultra-wideband diversity antenna, IEEE Trans. Antennas Propag. 57 (2009) 1597–1605.

[3] R. Kumar, N. Kushwaha, Design and investigation of sectoral circular disc monopole fractal antenna and its backscattering, Eng. Sci. Technol., An Int. J. 20 (2017) 18–27.

[4] Landolsi MA. Signal design for improved multiple access capacity in DS - UWB communication. Wirel Pers Commun. 2015;80(1):1 - 15.

[5] Batra A, Balakrishnan J, Aiello GR, Foerster JR, Dabak A. Design of a multiband OFDM system for realistic UWB channel environments. IEEE Trans Microwave Theory Tech. 2004;52(9):2125 - 2138.

[6] Chihi H, Bouallegue, R. Energy efficiency investigation for the MB - OFDM UWB cross - layer design. Wirel Pers Commun. 2017.

[7] A.-B. Zhang,C.-D. Kim, E. Yamada, F.G. Smith, The numerical investigation on the turbulent heat transfer, Int. J. Heat Mass Transfer 12: 345–365,2010.

[8] M.S. Sharawi, Current misuses and future prospects for printed multiple-input, multiple-output antenna systems, IEEE Antennas Propag. Mag. 59 (2017) 162– 170.

[9] D. Abed, H. Kimouche and B. Atrouz, Small-size printed CPW-fed antenna for ultra-wideband communications Elec. Lett., vol. 44, no. 17 pp. 2008

[10] H. Kimouche, D. Abed, B. Atrouz, and R. Aksas, "Bandwidth enhancement of rectangular monopole antenna using modified semi-elliptical ground plane and slots," Microw. Opt. Technol. Lett., vol. 52, no. 1, pp. 54–58, Jan. 2010.

[11] Federal Communications Commission, First Order and Report, Revision of Part 15 of the Commission's Rules Regarding UWB Transmission Systems, FCC 02–48, April 22, 2002.

[12] A. Najam, Y. Duroc, and S. Tedjni, "UWB-MIMO antenna with novel stub structure," Prog. Electromagn. Res. C, vol. 19, no. December 2010, pp. 245–257, 2011.

[13] A. Iqbal, O. A. Saraereh, A. W. Ahmad, and S. Bashir, "Mutual Coupling Reduction Using F-Shaped Stubs in UWB-MIMO Antenna," IEEE Access, vol. 6, pp. 2755–2759, 2017.

[14] M. S. Khan, M. F. Shafique, A. D. Capobianco, E. Autizi, and I. Shoaib, "Compact UWB-MIMO antenna array with a novel decoupling structure," Proc. 2013 10th Int. Bhurban Conf. Appl. Sci. Technol. IBCAST 2013, pp. 347–350, 2013.

[15] A. H. Jabire, H. X. Zheng, A. Abdu, and Z. Song, "Characteristic mode analysis and design of wide band MIMO antenna consisting of metamaterial unit cell," Electron., vol. 8, no. 1, 2019.

[16] A. Toktas, "G-shaped band-notched ultra-wideband MIMO antenna system for mobile terminals," IET Microwaves, Antennas Propag., vol. 11, no. 5, pp. 718–725, 2017.

[17] N. Malekpour and M. A. Honarvar, "Design of high-isolation compact MIMO antenna for UWB application," Prog. Electromagn. Res. C, vol. 62, no. December 2015, pp. 119–129, 2016.

[18] W. Li, Y. Hei, P. M. Grubb, X. Shi, and R. T. Chen, "Compact inkjet-printed flexible MIMO antenna for UWB applications," IEEE Access, vol. 6, pp. 50290–50298, 2018.

[19] G. Srivastava and A. Mohan, "Compact MIMO Slot Antenna for UWB Applications," IEEE Antennas Wirel. Propag. Lett., vol. 15, no. c, pp. 1057–1060, 2016.

[20] W. A. E. Ali and A. A. Ibrahim, "A compact double-sided MIMO antenna with an improved isolation for UWB applications," AEU - Int. J. Electron. Commun., vol. 82, pp. 7–13, 2017.

[21] S. I. Jafri, R. Saleem, M. F. Shafique, A. Brown, and A. K. Brown, "Compact reconfigurable multiple-input-multiple-output antenna for ultra wideband applications," IET Microwaves Antennas & Propagation. vol. 10, no. 4, pp. 413 – 419, 2016.

[22] Y. Zhao, F. S. Zhang, L. X. Cao, and D. H. Li, "A compact dual band-notched MIMO diversity antenna for UWB wireless applications," Prog. Electromagn. Res. C, vol. 89, no. December 2018, pp. 161–169, 2019.

[23] B. Azarm, J. Nourinia, C. Ghobadi, M. Majidzadeh, and N. Hatami, "A compact wimax band-notched UWB MIMO antenna with high isolation," Radioengineering, vol. 27, no. 4, pp. 983–989, 2018.

[24] W. T. Li, Y. Q. Hei, H. Subbaraman, X. W. Shi, and R. T. Chen, "Novel Printed Filtenna with Dual Notches and Good Out-of-Band Characteristics for UWB-MIMO Applications," IEEE Microw. Wirel. Components Lett., vol. 26, no. 10, pp. 765–767, 2016.

[25] L. Liu, S. W. Cheung, and T. I. Yuk, "Compact MIMO Antenna for Portable UWB Applications With Band-Notched Characteristic," IEEE Trans. Antennas Propag., vol. 63, no. 5, pp. 1917–1924, 2015.

[26] S. P. Biswal and S. Das, "A low-profile dual port UWB-MIMO/diversity antenna with band rejection ability," Int. J. RF Microw. Comput. Eng., vol. 28, no. 1, pp. 1–11, 2018.

[27] V. Bhanumathi and G. Sivaranjani, "High isolation MIMO antenna using semi-circle patch for UWB applications," Prog. Electromagn. Res. C, vol. 92, no. January, pp. 31–40, 2019.

[28] S. K. Yadav, A. Kaur, and R. Khanna, "Compact Rack Shaped MIMO Dielectric Resonator Antenna with Improved Axial Ratio for UWB Applications," Wirel. Pers. Commun., no. 0123456789, 2020.https://doi.org/10.1007/s11277-020-07887-x

[29] R. N. Tiwari, P. Singh, and B. K. Kanaujia, "A compact UWB MIMO antenna with neutralization line for WLAN/ISM/mobile applications," Int. J. RF Microw. Comput. Eng., vol. 29, no. 11, pp. 1–9, 2019.

[30] K. Srivastava, A. Kumar, B. K. Kanaujia, S. Dwari, and S. Kumar, "A CPW-fed UWB MIMO antenna with integrated GSM band and dual band notches," Int. J. RF Microw. Comput. Eng., vol. 29, no. 1, pp. 2–6, 2019.

[31] R. V. S. R. Krishna and R. Kumar, "Design and investigations of a microstrip fed open V-shape slot antenna for wideband dual slant polarization," Eng. Sci. Technol. an Int. J., vol. 18, no. 4, pp. 513–523, 2015.

[32] R. Yahya, A. Nakamura, M. Itami, and T. A. Denidni, "A Novel UWB FSS-Based Polarization Diversity Antenna," IEEE Antennas Wirel. Propag. Lett., vol. 16, no. c, pp. 2525–2528, 2017.

[33] R. V. R. Krishna, R. Kumar, and N. Kushwaha, "An UWB dual polarized microstrip fed L-shape slot antenna," Int. J. Microw. Wirel. Technol., vol. 8, no. 2, pp. 363–368, 2016.

[34] R.V.S. R. Krishna and R. Kumar, "A Dual-Polarized Square Ring Slot Antenna for UWB, Imaging and Radar Applications," IEEE Antennas and Wireless Propagation Letters, vol. 15, pp. 195 – 198, 2015.

[35] G. Saxena, P. Jain, and Y.K. Awasthi, "High Diversity Gain MIMO-Antenna for UWB Application with WLAN Notch Band Characteristic Including Human Interface Devices". Wireless Pers. Commun., vol., 112, pp.105–121, 2020. https://doi.org/10.1007/s11277-019-07018-1

[36] N. Ojaroudi Parchin, H. Jahanbakhsh Basherlou, Y. I A Al-Yasir, A. M Abdulkhaleq, and R. A Abd-Alhameed, "Ultra-Wideband Diversity MIMO Antenna System for Future Mobile Handsets," Sensors (Basel)., vol. 20, no. 8, pp. 1–19, 2020.

[37] K. V. Babu and B. Anuradha, "Design of UWB MIMO Antenna to Reduce the Mutual Coupling Using Defected Ground Structure," Wirel. Pers. Commun., no. 0123456789, 2021.

[38] Standard ECMA-368, "High Rate Ultra Wideband PHY and MAC Standard," 2008.

[39] E. Mehallel, D. Abed, A. Boukrouche, and A. Medjouri, "PAPR reduction in ECMA-368 UWB communication systems using parametric discrete sliding norm transform," Int. J. Commun. Syst., vol. 31, no. 17, 2018.

[40] L. Malviya, R. K. Panigrahi, and M. V. Kartikeyan, "MIMO antennas with diversity and mutual coupling reduction techniques: A review," Int. J. Microw. Wirel. Technol., vol. 9, no. 8, pp. 1763–1780, 2017.

[41] J. Foerster and Intel R&D, "Channel modelling sub-committee report final," IEEE P802.15 Working Group for Wireless Personal Area Networks (WPANs), IEEE P802.15-02/490r1-SG3a, Oct. 2005.

[42] D. Ghosh; A. De, M. C. Taylor, T. K. Sarkar, M. C. Wicks, and E. L. Mokole, "Transmission and Reception by Ultra-Wideband (UWB) Antennas," IEEE Antennas and Propagation Magazine (Vol. 48, no. 5, Oct. 2006)

[43] X. Qing, Z. N. Chen, and M. Y. W. Chia, "Characterization of ultrawideband antennas using transfer functions," Radio Sci., vol. 41, no. 1, pp. 1–10,

[44] Y. Duroc, A. Ghiotto, T. P. Vuong, and S. Tedjini, "UWB Antennas: Systems With Transfer Function and Impulse Response," IEEE transactions on antennas and propagation, vol. 55, no. 5, May 2007.

[45] P. Hallbjorner, "The significance of radiation efficiencies when using S-parameters to calculate the received signal correlation from two antennas", IEEE Antennas Wirel. Propag. Lett., vol. 4, pp. 97 - 99, 2005.

[46] M. S. Sharawi, "Current Misuses and Future Prospects for Printed Multiple-Input, Multiple-Output Antenna Systems," IEEE Ant. Prop. Mag., vol. 59, n. 2, pp. 97 - 99, 2017.